



HAL
open science

Age-related behavioural and striatal dysfunctions in Shank3 $\Delta C/\Delta C$ mouse model of autism spectrum disorder

Mathieu Thabault, Valentine Turpin, Éric Balado, Cloé Fernandes-Gomes, Anne-lise Huot, Anne Cantereau, Pierre-olivier Fernagut, Mohamed Jaber, Laurie Galvan

► To cite this version:

Mathieu Thabault, Valentine Turpin, Éric Balado, Cloé Fernandes-Gomes, Anne-lise Huot, et al.. Age-related behavioural and striatal dysfunctions in Shank3 $\Delta C/\Delta C$ mouse model of autism spectrum disorder. *European Journal of Neuroscience*, 2023, 57 (4), pp.607-618. 10.1111/ejn.15919 . hal-04028962

HAL Id: hal-04028962

<https://hal.science/hal-04028962>

Submitted on 15 Mar 2023

HAL is a multi-disciplinary open access archive for the deposit and dissemination of scientific research documents, whether they are published or not. The documents may come from teaching and research institutions in France or abroad, or from public or private research centers.

L'archive ouverte pluridisciplinaire **HAL**, est destinée au dépôt et à la diffusion de documents scientifiques de niveau recherche, publiés ou non, émanant des établissements d'enseignement et de recherche français ou étrangers, des laboratoires publics ou privés.



Distributed under a Creative Commons Attribution - NonCommercial - NoDerivatives 4.0 International License

RESEARCH REPORT

Age-related behavioural and striatal dysfunctions in $Shank3^{\Delta C/\Delta C}$ mouse model of autism spectrum disorder

Mathieu Thabault¹ | Valentine Turpin¹ | Éric Balado¹ |
 Cloé Fernandes-Gomes¹ | Anne-Lise Huot² | Anne Cantereau³ |
 Pierre-Olivier Fernagut¹ | Mohamed Jaber^{1,4}  | Laurie Galvan¹ 

¹Laboratoire de Neurosciences Expérimentales et Cliniques, Inserm, Université de Poitiers, Poitiers, France

²PREBIOS, Université de Poitiers, Poitiers, France

³IMAGE-UP, Université de Poitiers, Poitiers, France

⁴Centre Hospitalier Universitaire de Poitiers, Poitiers, France

Correspondence

Laurie Galvan, Laboratoire de Neurosciences Expérimentales et Cliniques, Inserm, Université de Poitiers, Poitiers, France.
 Email: laurie.galvan@univ-poitiers.fr

Funding information

Fondamental Foundation; CPER-FEDER program of the Région Nouvelle Aquitaine

Edited by: Eilís Dowd

Abstract

Autism spectrum disorders (ASDs) are defined as a set of neurodevelopmental disorders and a lifelong condition. In mice, most of the studies focused on the developmental aspects of these diseases. In this paper, we examined the evolution of motor stereotypies through adulthood in the $Shank3^{\Delta C/\Delta C}$ mouse model of ASD, and their underlying striatal alterations, at 10 weeks, 20 weeks, and 40 weeks. We highlighted that motor stereotypies worsened at 40 weeks possibly carried by earlier striatal medium spiny neurons (MSN) alterations in GABAergic transmission and morphology. Moreover, we report that 20 weeks could be a critical time-point in the striatal-related ASD physiopathology, and we suggest that MSN alterations may not be the direct consequence of developmental issues, but rather be a consequence of other impairments occurring earlier.

KEYWORDS

aging, ASD, MSN, $Shank3^{\Delta C/\Delta C}$, striatum

1 | INTRODUCTION

Autism spectrum disorder (ASD) represents chronic neurodevelopmental disorders characterized by the DSM-V by persistent deficits in communication and social

interactions, and restricted repetitive behaviours, interests, or activities (American Psychiatric Association, 2013). Even though motor symptoms are not considered as core symptoms, 88.2% of ASD patients undergo motor disabilities, and the risk factor of developing motor dysfunctions

Abbreviations: 10w, 10 weeks; 20w, 20 weeks; 40w, 40 weeks; ACSF, artificial cerebrospinal fluid; AMPA, alpha-amino-3-hydroxy-5-methyl-4-isoxazolepropionic acid; AP-V, (2R)-amino-5-phosphonovaleric acid; ASD, autism spectrum disorder; Bic, bicuculline; BSA, bovine serum albumin; Chd8, chromodomain helicase DNA binding protein 8; CNQX, cyanquinoxaline; DLS, dorsolateral striatum; DSM-V, Diagnostic and Statistical Manual of Mental Disorders, Fifth Edition; Fmr1, fragile X messenger ribonucleoprotein 1; GABA, gamma-amino butyric acid; GMO, genetically modified organism; KO, knock-out; MSN, medium spiny neuron; NL3, neuroligin 3; NMDA, N-methyl-D-aspartic acid; PBS, phosphate buffer saline; PCR, polymerase chain reaction; PSD-93/95, post-synaptic density 93/95; SAPAP3, DLG associated protein 3; SFARI, Simons Foundation Autism Research Initiative; Shank3, SH3 and multiple ankyrin repeat domains 3; sIPSC, spontaneous inhibitory post-synaptic current; WT, wild-type.

This is an open access article under the terms of the [Creative Commons Attribution-NonCommercial-NoDerivs](https://creativecommons.org/licenses/by-nc-nd/4.0/) License, which permits use and distribution in any medium, provided the original work is properly cited, the use is non-commercial and no modifications or adaptations are made.

© 2023 The Authors. *European Journal of Neuroscience* published by Federation of European Neuroscience Societies and John Wiley & Sons Ltd.

is fold by 22.2 between ASD patients and healthy population (Bhat, 2021). Thus, ASD-related motor disabilities severity seems to be proportionate to ASD core symptoms severity (for review, Zampella et al., 2021). As motor stereotypies are at the crossroads of stereotyped and motor behaviour, they represent a robust index of ASD symptom severity (Varghese et al., 2017).

Motor networks involve many brain structures, among which the striatum plays a central role as it controls sensorimotor coordination, gait, balance, and posture (Lanciego et al., 2012; Obeso et al., 2008). Two imaging studies have revealed that the putamen and caudate nucleus volumes are increased in ASD patients compared with age-matched control subjects (Hollander et al., 2005; Wegiel et al., 2014), with one of them reporting that the right caudate volume correlates with the magnitude of repetitive and stereotyped behaviours (Hollander et al., 2005). These neuroanatomical alterations are also recapitulated in some animal models of ASD with a larger striatum described in Neuroligin3 Knock-In mice (15 weeks) and in Cntnap2 Knock-Out (8–9 weeks) and Shank3 Knock-Out mice (22–23 weeks) (for review, Ellegood & Crawley, 2015). However, deeper understanding of striatal involvement in ASD symptoms and dysfunctions is needed, as ASD-related striatal data in patients and animal models are sparse (for review, Thabault et al., 2022).

Even though ASD has clearly a neurodevelopmental onset, these are lifelong conditions and are carried during adulthood and elderhood (Happé & Charlton, 2011). Life expectancy of ASD patients is reduced by nearly 17 years compared with the general population, partially due to their worsening comorbidities regardless of gender and level of functioning (Hirvikoski et al., 2016). Furthermore, aging ASD patients develop more neurological diseases and psychiatric disorders than neurotypical individuals (Hirvikoski et al., 2016; Jokiranta-Olkonemi et al., 2021). In mice, most studies focus on neurodevelopmental states or juvenile periods (6 and 12 weeks), and only a few explored the ASD pathophysiology in mature adults (20 to 30 weeks) (Kouser et al., 2013; Peñagarikano et al., 2011) and none in aging animals. This leaves a gap in knowledge of age-related ASD symptoms and in the evolution of ASD symptoms.

Shank3 is a gene coding for a synaptic scaffolding protein, and several mutations have been linked to ASD cases, making it a high confidence susceptibility ASD gene (SFARI database, <https://www.sfari.org/resource/sfari-gene/>). The *Shank3^{ΔC/ΔC}* mouse model correspond to the deletion of exon 21 resulting in the truncation of the C-terminal tail of the protein making it non-functional (Kouser et al., 2013). Several studies have shown that young adult *Shank3^{+ΔC}* and *Shank3^{ΔC/ΔC}*

mice exhibit core symptoms of ASD, such as impaired social recognition and communication, and stereotypies (Bidinosti et al., 2016; Duffney et al., 2015; Kouser et al., 2013; Matas et al., 2021). These mice also display ASD-like behaviours such as inflexibility, fear of novelty, without showing anxiety disorders (Bidinosti et al., 2016; Kouser et al., 2013). Interestingly, *Shank3* is highly expressed in the striatum, and *Shank3* knock-out (KO) leads to a decrease of striatal post synaptic proteins (SAPAP3, Homer, PSD-95, and PSD-93), an increase in neuronal arborization complexity but also a decrease in the cortico-striatal neurotransmission in 5- to 6-week-old mice (Peça et al., 2011). Although an increasing number of alterations in young *Shank3* mice are described, how these alterations evolve over time remain unknown. This is highly relevant for the pathophysiology of ASD as the disease is maintained with aging (Noone et al., 2006).

In this study, we investigated repetitive and exploratory motor behaviour and striatal dysfunctions in *Shank3* KO and control littermate at 10 weeks (10w, young adult), 20 weeks (20w, mature adult) and 40 weeks (40w, aged adult) in both genders.

2 | METHODS

2.1 | Animals

All experimental procedures were performed according to the Helsinki declaration and the guidelines of the European Union directive 2010/63/EU on the protection of animals used for scientific purposes. A local Ethics Committee approved all planned experiments (authorization no. 2018071316534636 and 2022021616096740). All experiments have been performed on both males and females, aged between 10 and 40 weeks, with the genetically modified organism (GMO) authorization #4231 from the French government. *Shank3^{+ΔC}* mice with a C-terminal deletion of *Shank3* at exon 21 (*Shank3tm1.1Pfw/J*) were obtained from Jackson laboratories and are on a C57BL/6J genetic background (Jackson Laboratories, USA). *Shank3^{+ΔC}* mice were mated to generate mice of all three genotypes: *Shank3^{+/+}* (WT), *Shank3^{+ΔC}*, and *Shank3^{ΔC/ΔC}* (KO). Sex and age-matched pups were separated from the dams on postnatal day 28 (P28) and were raised by groups of 3 to 5. Mice were genotyped by PCR using the following primers: common forward 5' GTG TCC CCT CAT TGA TGT TG 3', WT reverse 5' ATG TCC TGT TGCAGG TAG GG 3' and mutant reverse 5' GTC TGC CAC CTT CTG CCT AC 3'. All littermates were housed with an appropriate dark/light cycle, 12 h of each and had access to food and water ad libitum. Mice from the three genotypes were

segregated in three groups: young adult (10 weeks), mature adult (20 weeks), and aged adult (40 weeks).

2.2 | Behavioural analysis

Mice were acclimated for 10 min before filming to transparent Plexiglas cylinders (12 cm diameter) with minimal bedding to avoid digging. Each cylinder was separated by opaque sheets to isolate each mouse. Mice were then videotaped using VideoTrack[®] (ViewPoint[™], Lyon, France), and data were analysed with Solomon Coder[®] (András Péter, Keele, UK) by experimenters blind to both age and genotype. Grooming and rearing episodes were quantified for both number of episodes and total duration. For behavioural analysis, males and females were used as described in Table 1.

2.3 | Brain slice electrophysiology

Mice were deeply anaesthetized with diluted pentobarbital (120 mg/kg, Vetoquinol, Lure, France) and perfused transcardially with a high sucrose slicing solution containing (in mM): 208 sucrose, 10 glucose, 1.25 NaH₂PO₄·H₂O monobasic, 26 NaHCO₃, 2.5 KCl, 1.3 MgCl₂, and 8 MgSO₄ (pH 7.2–7.35, osmolality 290–310 mOsm/L). Mice were then decapitated, and brains were taken out of the skull and immediately placed in oxygenated (95%/5% O₂/CO₂) high sucrose slicing solution. Coronal slices (300 μm) were cut using a vibratome (Leica VT1200S, Leica camera AG, Wetzlar, Germany) and transferred into an incubating chamber containing artificial cerebrospinal fluid (ACSF) containing (in mM): 130 NaCl, 10 glucose, 1.25 NaH₂PO₄·H₂O monobasic, 26 NaHCO₃, 3 KCl, 2 MgCl₂, and 2 CaCl₂, oxygenated with 95%/5% O₂/CO₂ (pH 7.2–7.35, osmolality 290–310 mOsm/L). Slices were let to recover in ACSF for 1 h at room temperature before recordings.

MSN were identified using an upright microscope (Eclipse FN1, Nikon, Tokyo, Japan) at 40× magnification (40× Aplanachromat, Nikon, Tokyo, Japan) with infrared filter and monochromatic camera with Q-CapturePro[®]

TABLE 1 Males and females repartition in groups for behavioural analysis.

	WT		KO	
	Males	Females	Males	Females
10w	6	4	5	6
20w	7	6	8	3
40w	6	4	3	7

software (QImaging[™], Surrey, Canada). Whole-cell patch clamp recordings were performed at room temperature and were obtained using a MultiClamp 700B Amplifier, the Digidata 1440A digitizer, and the Clampex acquisition software (pCLAMP, Axon Instruments Inc. Molecular Devices, San José, CA). A maximum of two neurons per mouse per group were recorded.

Borosilicate patch pipettes (Harvard Apparatus, Holliston, MA), with resistance from 4 to 6 MΩ were pulled using a micropipette puller system (Flaming/Brown[™], Sutter Instrument Company, Novato, CA). Voltage-clamp experiments were performed with pipettes containing a caesium-based internal solution containing (in mM): 8 HEPES, 9 EGTA, 125 caesium-methanesulfonate, 4 NaCl, 3 KCl, 1 MgCl₂, 10 phosphocreatine-disodium, 0.1 Leupeptin, 5 Mg ATP, and 1 GTP Tris (pH 7.2, osmolality 270–280 mOsm/L). Membrane capacitance, resistance, and time constant were measured prior any recording. Inhibitory postsynaptic currents were recorded at +10 mV for 4 min, in presence of 10 μM CNQX and 50 μM AP-V (Tocris Bioscience[™], Bristol, UK). Finally, 10 μM bicuculline (Tocris Bioscience[™], Bristol, UK) was added to the flowing ACSF to block GABA-A receptors. Signal were pre-analysed with Clampfit software (v10.2, Axon Instruments Inc. Molecular Devices, San José, CA) and analysed with Minianalysis (Synaptosoft Inc., Fort Lee, NJ). Current-clamp recordings were performed using pipettes containing a potassium gluconate-based solution containing (in mM): 112.5 potassium-D-gluconate, 10 HEPES, 5 EGTA, 4 NaCl, 17.5 KCl, 0.5 CaCl₂, 1 MgCl₂, 5 ATP-dipotassium, and 1 GTP sodium salt (pH 7.19–7.24, osmolality 270–280 mOsm/L). All internal electrode solutions contained 0.2% biocytin for subsequent detection of recorded cells.

2.4 | Drugs

For electrophysiological recordings, drugs (Tocris Bioscience[™], Bristol, UK) were dissolved in H₂O and stock solutions were as following: 50 mM D-2-amino-5-phosphonovalerate (AP-V, Ref 0106), 10 mM cyanquixaline (CNQX, Ref 1045), and 20 mM bicuculline methiodide (Bic, Ref 2503). AP-V was used at a working concentration of 50 μM, and CNQX and Bic were used at a working concentration of 10 μM.

2.5 | Neuronal morphology analysis

All patched slices were incubated in 4% paraformaldehyde (PFA) solution overnight for tissue fixation and

transferred in a cryoprotective 20% sucrose solution, prior to use for fluorescence detection of recorded cells. All steps were performed at room temperature, except streptavidin incubation times that was completed at 4°C. Tissue sections were washed twice for 5 min using 1× phosphate buffer saline (PBS). One hour bath in 1× PBS + 1% bovine serum albumin (BSA) + 0.2% Triton allowed then to permeabilize the slices and to block non-specific fixation sites. Slices were left to incubate overnight at 4°C with Alexa 488 conjugated streptavidin (1:1000) in blocking solution and covered to avoid photobleaching. Slices were washed with three baths of 5 min in 1× PBS and then set on glass slides and left to dry. Slides were briefly immersed in toluene and then mounted using DePeX™ (Thermo Fisher Scientific, Inc., Waltham, MA) prior to storage at 4°C. Images were acquired with the confocal microscope OLYMPUS FV3000 (Olympus Europa SE & Co. KG, Hamburg, Germany) and analysed using IMARIS software suite (IMARIS v9.8.2, Oxford Instruments, Abington, Oxon, UK). Dendritic spines were sorted using specific criteria (see Table 2) and analysed according to the level of dendritic branch to which they are connected.

TABLE 2 Spine sorting criteria.

		Criterion 1 – Spine length (µm)	
		≤0.75	>0.75
Criterion 2 – Ratio diameter head/neck	≤1	Stubby	Thin
	>1	Mushroom	Mushroom

Note: Adapted from Hering and Sheng (2001), Pchitskaya and Bezprozvanny (2020) and Sebastian et al. (2013).

2.6 | Statistical analysis

Data in boxplots are expressed as median and min–max, and ‘+’ stands for the mean. All other data are expressed as mean ± standard error of the mean (SEM). Statistics were performed with Prism® (v9.0.0, GraphPad™ Software Inc., La Jolla, CA), and graphs were made with Prism®. Appropriate statistical tests are mentioned under each figure, and results were considered as significantly different for $p < 0.05$. All figures were made with Corel Draw X7® (v17.2.0.688, Corel™ Corporation, Ottawa, Canada).

3 | RESULTS

3.1 | Grooming behaviour increases with aging in Shank3 KO mice contrary to the rearing behaviour that shows an opposite change

To determine how motor stereotypies evolve with aging, we quantified grooming behaviour in both WT and

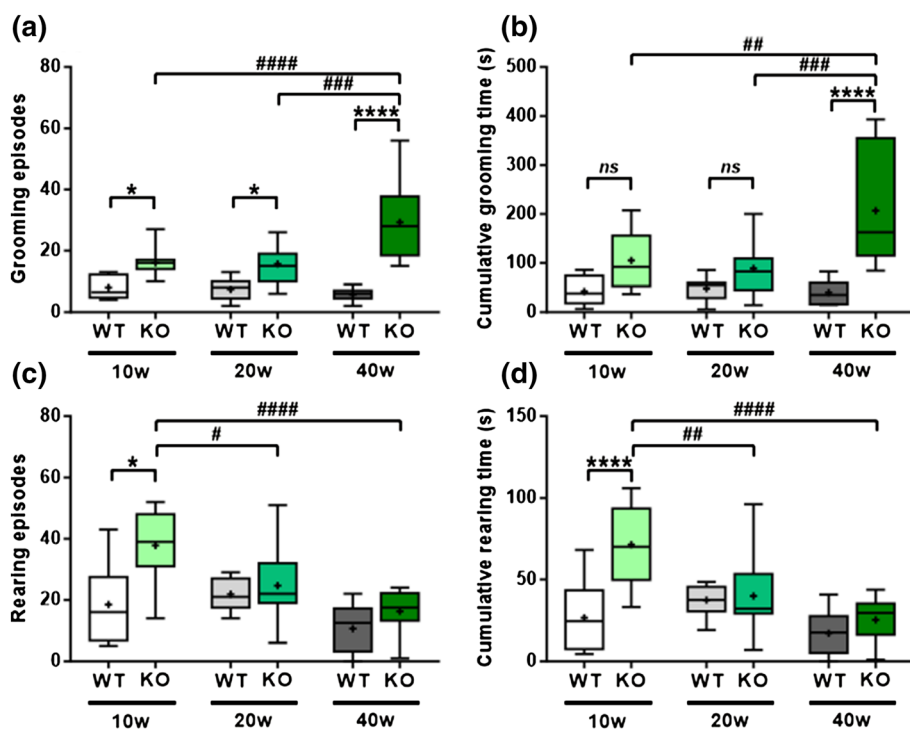


FIGURE 1 Age-related modifications of the behavioural output in Shank3 KO mice. (a) Grooming frequency (left) and cumulative time (right). (b) Rearing frequency (left) and cumulative time (right). (c) Global behavioural output measured in Shank3 WT and KO mice. Two-way ANOVA, Tukey post hoc. * = genotype effect; # = age effect. Sidak post hoc for behavioural difference * $p < 0.05$, ** $p < 0.01$, **** $p < 0.0001$. Number of mice: $N = 10$ WT 10w, $N = 11$ KO 10w, $N = 13$ WT 20w, $N = 11$ KO 20w, $N = 10$ WT 40w, $N = 10$ KO 40w.

Shank3 KO mice at 10w, 20w, and 40w. As we did not find differences between males and females in each group, data from both genders were pooled. The 10w KO mice displayed excessive grooming behaviour ($F_{(2,59)} = 10.72$, $p = 0.0001$, Tukey WT_{10w} vs. KO_{10w} $p = 0.0495$, Figure 1a) compared with WT littermate. This phenotype was maintained at 20w (WT_{20w} vs. KO_{20w} $p = 0.0224$) and worsened at 40w. Indeed, the 40w KO mice drastically displayed more grooming episodes with aging (KO_{10w} vs. KO_{40w} $p = 0.0001$, KO_{20w} vs. KO_{40w} $p < 0.0001$). Also, the cumulative grooming duration increased at this stage ($F_{(2,59)} = 5.386$, $p = 0.0071$, Tukey KO_{10w} vs. KO_{40w} $p = 0.0035$, KO_{20w} vs. KO_{40w} $p = 0.0005$). Rearing behaviour, reflecting exploratory behaviour, was also assessed during this test. As early as 10 weeks, the KO mice displayed excessive rearing behaviour ($F_{(2,59)} = 12.51$, $p < 0.0001$, Tukey WT_{10w} vs. KO_{10w} $p = 0.0003$) compared with WT mice, suggesting that they experienced stress-induced hyperactivity. The rearing behaviour was then no longer excessive at 20w, while the grooming behaviour was still excessive.

3.2 | The 20-week-old Shank3 KO MSN displayed neurotransmission changes

As motor stereotypies and more generally motor behaviour are linked with the dorsolateral striatum (DLS), we aimed at recording DLS MSN *ex vivo* to assess whether behavioural modifications with aging were linked to MSN dysfunctions. We first measured MSN intrinsic

passive membrane properties (Table 3). Although neither membrane capacitance nor membrane resistance exhibited a difference with aging in both groups, the time constant was decreased in an age-related manner in both groups ($F_{(2,40)} = 8.230$, $p = 0.0010$). However, changes occurred at different stages: in WT mice, the time constant decreased with aging between 10w and 40w (-34.78% , $p = 0.0213$), while in KO mice, it decreased between 20w and 40w (-31.82% , $p = 0.0069$) suggesting a difference in the aging process. No modifications in resting membrane potential nor in action potential (AP) parameters (number of AP, amplitude, rheobase, kinetics, threshold, and hyperpolarization duration and amplitude) were observed among groups.

As intrinsic MSN properties and excitability did not show drastic changes, we next explored GABAergic inputs onto the DLS MSN, by recording spontaneous inhibitory postsynaptic currents (IPSC) in presence of glutamatergic blockers, an index of striatal GABAergic environment. At 10w, neither of the measured parameters were altered in KO mice compared with WT. Interestingly, at 20w, we observed an increase of small amplitude events (10–15 pA) (age-effect: $F_{(10,400)} = 14.76$, $p < 0.0001$, Tukey WT_{20w} vs. KO_{20w} $p = 0.0002$). There was also a significant difference in the cumulative interevent interval distribution between WT and KO mice at 20w, from 500 to 2000 ms, suggesting an increase in GABA release probability ($F_{(50,2000)} = 529.8$, $p < 0.0001$) in KO mice compared with WT (Figure 2b). The IPSC frequency was significantly increased in KO 20w MSN ($U = 14$, $p = 0.0268$) compared WT MSN

TABLE 3 Time constant is differentially altered in an age-dependent manner in WT and KO mice.

		Capacitance (pF)		Resistance (MΩ)		Time constant (ms)		Resting potential (mV)			
		Mean	± SEM	Mean	± SEM	Mean	± SEM	Mean	± SEM		
10w	WT ($n = 7$)	100.7	± 7.2	142.7	± 14.2	2.3	± 0.1	}	-79.6	± 3.5	$n = 6$
	KO ($n = 7$)	87.9	± 6.5	154.4	± 12.3	1.9	± 0.1		-78.0	± 2.5	$n = 7$
20w	WT ($n = 7$)	78.7	± 11.9	125.7	± 16.6	1.8	± 0.1	}	-82.7	± 3.0	$n = 7$
	KO ($n = 11$)	91.5	± 11.1	166.5	± 14.0	2.2	± 0.2		-80.7	± 4.0	$n = 10$
40w	WT ($n = 6$)	79.2	± 5.1	146.0	± 13.4	1.5	± 0.1	}	-74.9	± 3.8	$n = 8$
	KO ($n = 8$)	86.1	± 12.6	154.8	± 21.4	1.5	± 0.1		-80.7	± 3.3	$n = 11$

Note: Membrane capacitance and resistance and time constant were measured with Cs-based internal solution. Resting membrane potential was measured with K-Gluconate based internal solution. Two-way ANOVA, Tukey post hoc. # = age effect. Number of mice/neurons: $N/n = 5/7$ WT 10w, $N/n = 6/7$ KO 10w, $N/n = 6/7$ WT 20w, $N/n = 7/11$ KO 20w, $N/n = 6/6$ WT 40w, $N/n = 8/8$ KO 40w neurons.

$p < 0.05$.

$p < 0.01$.

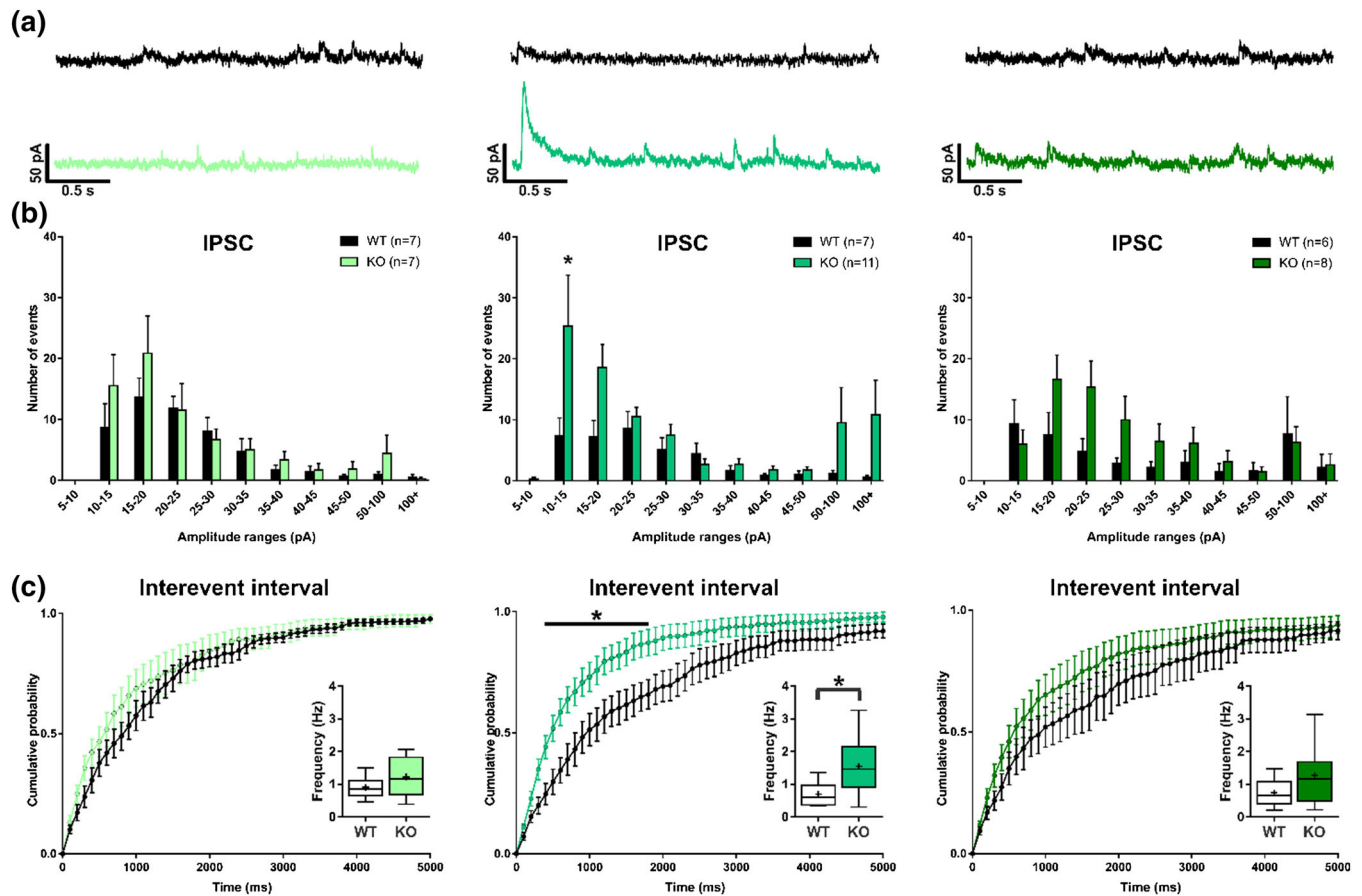


FIGURE 2 IPSC frequency alterations with aging in KO mice. (a) Representative traces of IPSCs recording of DLS MSN at 10w (left), 20w (middle), and 40w (right). (b) Distribution of the number of IPSC across the IPSC amplitude (bin = 5 pA). (c) Interevent intervals with IPSC frequency in inserts. Two-way ANOVA, Tukey post hoc. * = genotype effect, $p < 0.05$. Number of mice/neurons: $N/n = 5/7$ WT 10w, $N/n = 6/7$ KO 10w, $N/n = 6/7$ WT 20w, $N/n = 7/11$ KO 20w, $N/n = 6/6$ WT 40w, $N/n = 8/8$ KO 40w.

suggesting an increase at the presynaptic level. Interestingly, that difference was not observed by 40w, suggesting that 20w could be a critical time for striatal dysfunction implementation in this ASD model.

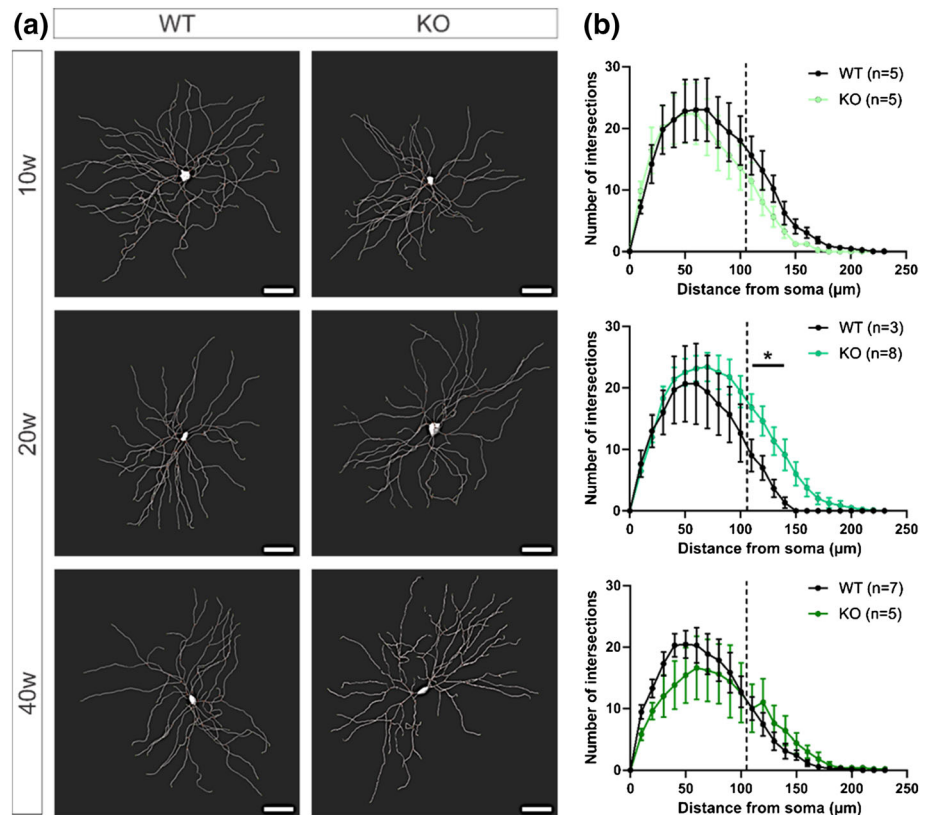
3.3 | Shank3 KO MSN morphology is altered in aged animals

To understand whether the observed neurotransmission dysfunctions were linked to neuronal morphological changes, we assessed MSN dendritic arborization using Sholl analysis (Figure 3). Their distal arborization was significantly denser in KO mice than in WT mice at 20w only ($F_{(12,324)} = 69.59$, $p < 0.0001$), at 110 μm ($p = 0.0146$), 120 μm ($p = 0.0173$), 130 μm ($p = 0.0154$), and 140 μm ($p = 0.0138$), suggesting that morphological adaptive mechanisms could occur at this stage.

As MSN receives the main part of their inputs onto dendritic spines, we next examined the dendritic spine

density on third, fourth, and fifth level dendrites (Figure 4a), highlighting effects of age for each of them (Level 3 $F_{(2,193)} = 14.86$, $p < 0.0001$, Tukey WT_{10w} vs. WT_{20w} $p = 0.0029$, KO_{10w} vs. KO_{40w} $p < 0.0001$, KO_{20w} vs. KO_{40w} $p = 0.0206$. Level 4 $F_{(2,201)} = 18.63$, $p < 0.0001$, Tukey WT_{10w} vs. WT_{20w} $p < 0.0001$, WT_{20w} vs. WT_{40w} $p = 0.0272$, KO_{10w} vs. KO_{40w} $p < 0.0001$. Level 5 $F_{(2,150)} = 5.046$, $p = 0.0076$, Tukey WT_{10w} vs. WT_{20w} $p = 0.0209$, WT_{20w} vs. WT_{40w} $p = 0.0003$). Spine density was also significantly decreased between WT and KO mice at 40w for fourth and fifth dendritic levels (Level 4 $F_{(1,201)} = 8.135$, $p = 0.0048$, Tukey WT_{40w} vs. KO_{40w} $p < 0.0001$. Level 5 $F_{(1,150)} = 7.278$, $p = 0.0078$, Tukey WT_{40w} vs. KO_{40w} $p = 0.0002$). These data suggest again that aging processes could be different between WT and KO mice. To identify whether these changes in spine density were supported by changes in density of shape-specific spines, we sorted spines into three groups: thin, mushroom, and stubby spines as described in Table 1. We highlighted that age-related decreases of spine

FIGURE 3 MSN dendritic arborization is increased at 20w in KO mice. (a) Representative neuronal morphology obtained with IMARIS software. Scale bar 40 μ m. (b) Sholl analysis of the MSN arborization density. Two-way ANOVA, Tukey post hoc. * = genotype effect, * $p < 0.05$. Number of mice/neurons: $N/n = 4/5$ WT 10w, $N/n = 5/5$ KO 10w, $N/n = 2/3$ WT 20w, $N/n = 6/8$ KO 20w, $N/n = 8/8$ WT 40w, $N/n = 5/5$ KO 40w.



density onto third level dendrites are mainly due to decreases of thin and mushroom spine density (Figure 4b–d) (Thin $F_{(2,198)} = 15.54$, $p < 0.0001$, Tukey WT_{10w} vs. WT_{20w} $p < 0.0001$, KO_{10w} vs. KO_{40w} $p = 0.0021$, KO_{20w} vs. KO_{40w} $p < 0.0001$. Mushroom $F_{(2,198)} = 78.38$, $p < 0.0001$, Tukey WT_{10w} vs. WT_{20w} $p < 0.0001$, KO_{10w} vs. KO_{40w} $p < 0.0001$, KO_{20w} vs. KO_{40w} $p = 0.0007$) suggesting that these modifications are independent of the spine maturity stages. For fourth and fifth level dendrites, we highlighted that changes in density of all three spine types seem to account for global spine density variations with aging (Level 4 Thin $F_{(2,247)} = 49.64$, $p < 0.0001$. Mushroom $F_{(2,247)} = 109.2$, $p < 0.0001$. Stubby $F_{(2,247)} = 24.7$, $p < 0.0001$. Level 5 Thin $F_{(2,156)} = 32.04$, $p < 0.0001$. Mushroom $F_{(2,156)} = 144.6$, $p < 0.0001$. Stubby $F_{(2,156)} = 14.5$, $p < 0.0001$). However, the fall of spine density between WT and KO mice at 40w seems to be due to the fall of thin and stubby spines only, suggesting here that mature spines are preserved on fourth and fifth level dendrites (Level 4 Thin $F_{(1,247)} = 28.31$, $p < 0.0001$ Tukey WT_{40w} vs. KO_{40w} $p < 0.0001$. Stubby $F_{(1,247)} = 47.49$, $p < 0.0001$ Tukey WT_{40w} vs. KO_{40w} $p < 0.0001$. Level 5 Thin $F_{(1,156)} = 20.17$, $p < 0.0001$ Tukey WT_{40w} vs. KO_{40w} $p < 0.0001$. Stubby $F_{(1,156)} = 45.23$, $p < 0.0001$ Tukey WT_{40w} vs. KO_{40w} $p < 0.0001$).

4 | DISCUSSION

In this paper we analysed the effects of aging on motor stereotypies and rearing behaviour, along with functionality and morphology of striatal medium spiny neurons, in the Shank3^{ΔC/ΔC} (KO) mouse model of ASD. We were interested in studying aging as ASD are a lifelong condition and a large part of clinical and animal studies focused on developmental stages. Thus, while social and associative symptoms are subject to interpretation and are often different from a context to another in humans (Nestler & Hyman, 2010), the motor stereotypies constitute a robust index of autistic spectrum (Varghese et al., 2017). In this study, we used KO animals and age-matched WT control littermates at 10w, 20w, and 40w, standing for young adult, adult, and old stages. We used groups gathering males and females as no sex-related differences have been statistically observed for behavioural analysis in our hands.

We demonstrated that motor stereotypies are present at 10w and 20w and worsened with aging at 40w in Shank3 KO mice compared with WT. While previous papers showed excessive grooming behaviour in these mice (10w, Matas et al., 2021; 40w, Kouser et al., 2013), we provide the first evidence of symptom worsening with aging. We also went further in the analysis as we

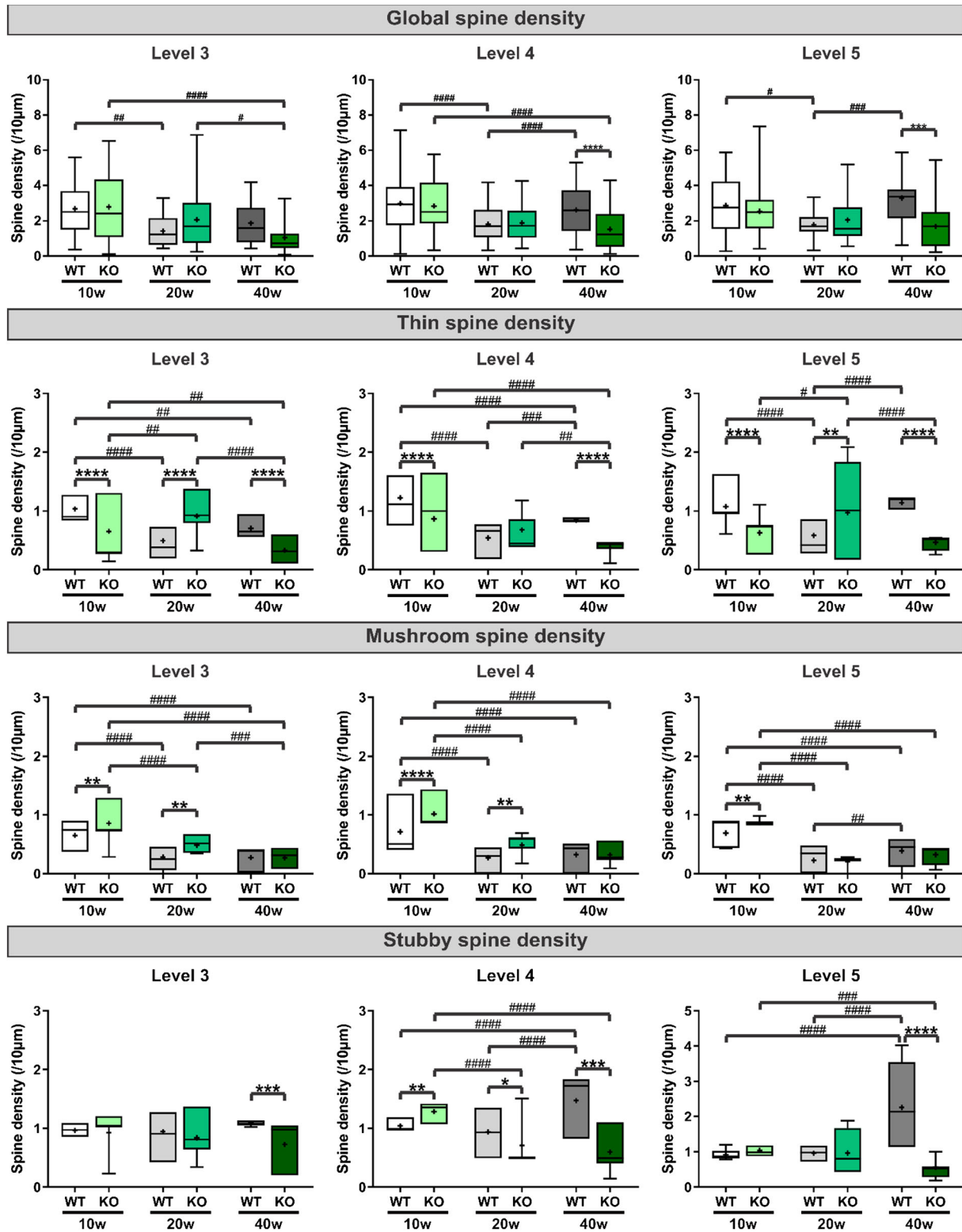


FIGURE 4 Dendritic spine density is altered with aging. (a) Global spine density, (b) thin spine density, (c) mushroom spine density, and (d) stubby spine density on third (left), fourth (middle), and fifth (right) level dendritic segments. Two-way ANOVA, Tukey post hoc. * = genotype effect, # = age effect; * $p < 0.05$, ** $p < 0.01$; *** $p < 0.001$; **** $p < 0.0001$. Number of labelled neuron/dendritic segments: Level 3 $N/n = 3/35$ WT 10w, $N/n = 3/28$ KO 10w, $N/n = 3/32$ WT 20w, $N/n = 4/51$ KO 20w, $N/n = 3/27$ WT 40w, $N/n = 3/31$ KO 40w segments. Level 4 $N/n = 3/51$ WT 10w, $N/n = 3/46$ KO 10w, $N/n = 3/53$ WT 20w, $N/n = 4/34$ KO 20w, $N/n = 3/39$ WT 40w, $N/n = 3/30$ KO 40w segments. Level 5 $N/n = 3/22$ WT 10w, $N/n = 3/36$ KO 10w, $N/n = 3/37$ WT 20w, $N/n = 4/16$ KO 20w, $N/n = 3/20$ WT 40w, $N/n = 3/32$ KO 40w.

investigated an intermediate time (20w) and we also included rearing behaviour as another component of the test. Rearing was excessive at 10w and progressively decreased at 20w and 40w, in parallel with an increase of grooming behaviour, leading to behavioural output alterations in KO mice at 40w. Taken together, these findings strongly suggest that in this model, 20w (adult stage) seems to be a turning point for behavioural evolution with aging, leading to global behavioural alteration at latter stages. These findings could partially reflect the symptoms and comorbidities worsening observed in some patients at adulthood including motor stereotypies (Croen et al., 2015; Jokiranta-Olkonemi et al., 2021; Noone et al., 2006; Schoufour et al., 2013).

The excitation/inhibition imbalance hypothesis of ASD (Nelson & Valakh, 2015; Rubenstein & Merzenich, 2003) has been extensively examined mainly for its excitatory part in the Shank3 models of ASD (Delling & Boeckers, 2021), as Shank3 protein is expressed at glutamatergic synapses in the striatum (Yoo et al., 2018). In this study, we focused on the dorsolateral striatum, which is directly linked to motor stereotypies (Hollander et al., 2005; Rojas et al., 2006). We examined the condition of local GABAergic transmission in this structure by recording (i) MSN intrinsic properties and (ii) spontaneous inhibitory post-synaptic currents on MSN. We first showed that the time constant Tau was reduced between 10w and 40w in WT mice and between 20w and 40w in KO mice, suggesting that there could be a delay in excitability alterations due to the Shank3 mutation and reinforcing the hypothesis that 20w could be a crucial time point in the evolution of the ASD-related impairments in KO mice. However, we were not able to determine whether the recorded neurons expressed the dopaminergic receptor D1 or D2, and so to identify their implication in the striato-nigral or striato-pallidal pathways. Given that the MSN excitability is slightly different between the two populations (Kreitzer & Malenka, 2007), this could be a limitation of our study and would need further exploration.

Our data clearly highlight that frequency and distribution of events are affected in KO mice at 20w only, resulting in a significant increase of the number of small amplitude currents (10–15 pA) as well as a trend to increase for high amplitude currents (50pA and more), leading to a significant increase of IPSC frequency and cumulative probability. Interestingly, neither the IPSC distribution, the cumulative probability nor the frequency was affected at younger stage (10w) or latter stage (40w), leading to the reinforcement of our 20w-shift hypothesis. These findings are a major step forward in the comprehension of the GABAergic related alterations in ASD models, as little is known about it (Thabault

et al., 2022). The first clear GABAergic involvement in ASD physiopathology is that transgenic mice lacking either alpha 5 or beta 3 GABA-A receptor subunit display ASD-like phenotypes (DeLorey, 2005; Zurek et al., 2016). To date, striatal GABAergic impairments are observed only in a few models of ASD, such as *Chd8*^{+/-} mice (Platt et al., 2017), *NL3-cKO* mice (Rothwell et al., 2014), and *Fmr1*^{-/-} mice (Centonze et al., 2008), but were never described in any *Shank3* model of ASD. Moreover, our findings provide the first evidence of age-related alterations in a murine model of ASD, as all above-cited studies used 4 weeks to 10 weeks mice.

It is now well established that dysfunctions in neurotransmission often go with neuronal morphological alterations (for example, in ASD: Peça et al., 2011, or in Huntington's disease: Holley et al., 2019). To explore this possibility, we performed a Sholl analysis to examine dendritic arborization. We report an increase of the distal dendritic arborization in KO mice at 20w only, with no changes in the proximal arborization. Interestingly, this increase in the MSN morphology has been previously described in another *Shank3* mouse model of ASD (Peça et al., 2011) but at younger stages (5–6w).

As morphological disturbances were highlighted on distal arborization, we next measured the dendritic spine density on third, fourth, and fifth level dendritic segments. Differences observed here were mainly a result of aging. Indeed, we showed that the global spine density is significantly lower in KO mice than in WT mice at 40w only, on the most distal dendritic segments. Interestingly, in the *Shank3B* KO mouse model of ASD, the spine density was reported to be decreased as early as 5–6w (Peça et al., 2011). This suggests that the deletion of the C-terminal part of the protein leads to age-dependent alterations of the spine density, but not at young stages. We then sorted the spines into three different groups: thin, stubby, and mushroom spines, according to previous studies (Hering & Sheng, 2001; Pchitskaya & Bezprozvanny, 2020; Sebastian et al., 2013). We found that in third level dendrites, the age-related changes in density can be attributed to changes in the density of thin and mushroom spines, which are, respectively, immature and mature spines (Pchitskaya & Bezprozvanny, 2020). However, although the stubby spine density is supposed to fall with aging (Bloss et al., 2011; Hering & Sheng, 2001), we observed this decrease on fourth and fifth dendritic segments only, where all three spine types are decreased with aging. Finally, the decrease of the spine density between WT and KO mice at 40w on most distal dendritic segments is carried by a fall in thin and stubby spine density, but not mushroom spine density, as also shown in aging studies (Bloss et al., 2011). Given that mushroom spine density is higher in KO mice than in

WT mice at 10w and 20w, we suggest that maturation but not maintenance of the dendritic spines could be affected in this murine model of ASD.

5 | CONCLUSION

Here, we highlighted that motor stereotypies worsen with aging in KO mice, at the expense of other behaviours like rearing behaviour. This worsening of ASD symptom at 40w seems to be due to earlier disturbances of the striatal GABAergic transmission and to MSN morphological impairments. Taken together, our findings suggest that MSN alterations in ASD may not constitute the primary consequence of developmental impairments but occur at later stages, possibly as a consequence of other alterations. Although neuronal plasticity accompanied by long-term synaptic remodelling occurs mostly in the developing brain, it can also be found in adulthood. In this study, our findings indicate that the 20w window seems to be a critical time point for MSN in ASD mice. We hypothesize that non-MSN cells could have been affected early during the neurodevelopmental process leading to abnormal striatal neurotransmission in ASD. These striatal dysfunctions could have been partially compensated from birth to the early life of the ASD mice by MSNs. At 20w, the MSN's initial compensatory mechanisms may not be enough to cope with the aggravated dysfunctions shifting to a new state with synaptic remodelling and resulting in altered MSN plasticity. This adult synaptic remodelling has been well-defined in the adult mouse visual cortex after a retinal lesion but not yet in the ASD striatum (for review, Hübener & Bonhoeffer, 2014; Keck et al., 2008). We speculate that these initial dysfunctional cells may be the striatal PV interneurons given their demonstrated implication in ASD (for review, Filice et al., 2020) and their action of feedforward inhibition onto MSNs that can control striatal calcium-dependent plasticity (Owen et al., 2018).

ACKNOWLEDGEMENTS

We thank all the Prebios Animal Facility staff for their help in animal care and the maintenance of the mouse lineage. We also thank Shana Sauzeau and Élisabeth Audouard for their implication in this project and their help in morphological analysis. We thank our financial supports: the Fondamental Foundation and the CPER-FEDER program of the Région Nouvelle Aquitaine.

CONFLICT OF INTEREST

The authors have no conflicts of interest.

AUTHOR CONTRIBUTIONS

Mathieu Thabault performed behavioural, electrophysiological and histological experiments and collected and analysed the data. Éric Balado designed behavioural test apparatus. Valentine Turpin and Cloé Fernandes-Gomes performed some behavioural experiments and collected and analysed the data. Mohamed Jaber provided Shank transgenic mouse line and partial financial support. Anne-Lise Huot maintained the mouse line and helped with animal welfare. Anne Cantereau performed confocal image acquisition. Laurie Galvan is the PI of the project. She designed the aims and obtained some of the financial grants study. Laurie Galvan and Pierre-Olivier Fernagut interpreted. Mathieu Thabault and Laurie Galvan wrote the manuscript. All authors reviewed the manuscript and approved the final version.

PEER REVIEW

The peer review history for this article is available at <https://publons.com/publon/10.1111/ejn.15919>.

DATA AVAILABILITY STATEMENT

Data supporting the findings of this study are available from the corresponding author, upon reasonable request.

ORCID

Mohamed Jaber  <https://orcid.org/0000-0003-2536-1913>

Laurie Galvan  <https://orcid.org/0000-0002-7851-0102>

REFERENCES

- American Psychiatric Association. (2013). Diagnostic and Statistical Manual of Mental Disorders. <https://doi.org/10.1176/appi.books.9780890425596>
- Bhat, A. N. (2021). Motor impairment increases in children with autism spectrum disorder as a function of social communication, cognitive and functional impairment, repetitive behavior severity, and comorbid diagnoses: A SPARK study report. *Autism Research, 14*(1), 202–219. <https://doi.org/10.1002/aur.2453>
- Bidinosti, M., Botta, P., Kröttner, S., Proenca, C. C., Stoehr, N., Bernhard, M., Fruh, I., Mueller, M., Bonenfant, D., Voshol, H., Carbone, W., Neal, S. J., McTighe, S. M., Roma, G., Dolmetsch, R. E., Porter, J. A., Caroni, P., Bouwmeester, T., Löthi, A., & Galimberti, I. (2016). CLK2 inhibition ameliorates autistic features associated with SHANK3 deficiency. *Science, 351*(6278), 1199–1203. <https://doi.org/10.1126/science.aad5487>
- Bloss, E. B., Janssen, W. G., Ohm, D. T., Yuk, F. J., Wadsworth, S., Saardi, K. M., McEwen, B. S., & Morrison, J. H. (2011). Evidence for reduced experience-dependent dendritic spine plasticity in the aging prefrontal cortex. *Journal of Neuroscience, 31*(21), 7831–7839. <https://doi.org/10.1523/JNEUROSCI.0839-11.2011>
- Centonze, D., Rossi, S., Mercaldo, V., Napoli, I., Ciotti, M. T., de Chiara, V., Musella, A., Prosperetti, C., Calabresi, P., Bernardi, G., & Bagni, C. (2008). Abnormal striatal GABA transmission in the mouse model for the fragile X syndrome.

- Biological Psychiatry*, 63(10), 963–973. <https://doi.org/10.1016/j.biopsych.2007.09.008>
- Croen, L. A., Zerbo, O., Qian, Y., Massolo, M. L., Rich, S., Sidney, S., & Kripke, C. (2015). The health status of adults on the autism spectrum. *Autism*, 19(7), 814–823. <https://doi.org/10.1177/1362361315577517>
- Delling, J. P., & Boeckers, T. M. (2021). Comparison of SHANK3 deficiency in animal models: Phenotypes, treatment strategies, and translational implications. *Journal of Neurodevelopmental Disorders*, 13(1) BioMed Central Ltd, 55. <https://doi.org/10.1186/s11689-021-09397-8>
- DeLorey, T. M. (2005). GABRB3 gene deficient mice: A potential model of autism spectrum disorder. *International Review of Neurobiology*, 71(5), 359–382. [https://doi.org/10.1016/S0074-7742\(05\)71015-1](https://doi.org/10.1016/S0074-7742(05)71015-1)
- Duffney, L. J., Zhong, P., Wei, J., Matas, E., Cheng, J., Qin, L., Ma, K., Dietz, D. M., Kajiwar, Y., Buxbaum, J. D., & Yan, Z. (2015). Autism-like deficits in Shank3-deficient mice are rescued by targeting actin regulators. *Cell Reports*, 11(9), 1400–1413. <https://doi.org/10.1016/j.celrep.2015.04.064>
- Ellegood, J., & Crawley, J. N. (2015). Behavioral and neuroanatomical phenotypes in mouse models of autism. *Neurotherapeutics*, 12(3), 521–533. <https://doi.org/10.1007/s13311-015-0360-z>
- Filice, F., Janickova, L., Henzi, T., Bilella, A., & Schwaller, B. (2020). The parvalbumin hypothesis of autism spectrum disorder. *Frontiers in Cellular Neuroscience*, 14(December), 577525. <https://doi.org/10.3389/fncel.2020.577525>
- Happé, F., & Charlton, R. A. (2011). Aging in autism spectrum disorders: A mini-review. *Gerontology*, 58(1), 70–78. <https://doi.org/10.1159/000329720>
- Hering, H., & Sheng, M. (2001). Dendritic spines: Structure, dynamics and regulation. *Nature Reviews Neuroscience*, 2, 880–888. www.nature.com/reviews/neuro, <https://doi.org/10.1038/35104061>
- Hirvikoski, T., Mittendorfer-Rutz, E., Boman, M., Larsson, H., Lichtenstein, P., & Bölte, S. (2016). Premature mortality in autism spectrum disorder. *British Journal of Psychiatry*, 208(3), 232–238. <https://doi.org/10.1192/bjp.bp.114.160192>
- Hollander, E., Anagnostou, E., Chaplin, W., Esposito, K., Haznedar, M. M., Licalzi, E., Wasserman, S., Soorya, L., & Buchsbaum, M. (2005). Striatal volume on magnetic resonance imaging and repetitive behaviors in autism. *Biological Psychiatry*, 58(3), 226–232. <https://doi.org/10.1016/j.biopsych.2005.03.040>
- Holley, S. M., Galvan, L., Kamdjou, T., Cepeda, C., & Levine, M. S. (2019). Striatal GABAergic interneuron dysfunction in the Q175 mouse model of Huntington's disease. *European Journal of Neuroscience*, 49(1), 79–93. <https://doi.org/10.1111/ejn.14283>
- Hübener, M., & Bonhoeffer, T. (2014). Neuronal plasticity: Beyond the critical period. In *Cell* (Vol. 159, issue 4) (pp. 727–737). Cell Press. <https://doi.org/10.1016/j.cell.2014.10.035>
- Jokiranta-Olkoniemi, E., Gyllenberg, D., Sucksdorff, D., Suominen, A., Kronström, K., Chudal, R., & Sourander, A. (2021). Risk for premature mortality and intentional self-harm in autism spectrum disorders. *Journal of Autism and Developmental Disorders*, 51(9), 3098–3108. <https://doi.org/10.1007/s10803-020-04768-x>
- Keck, T., Mrcic-Flogel, T. D., Vaz Afonso, M., Eysel, U. T., Bonhoeffer, T., & Hübener, M. (2008). Massive restructuring of neuronal circuits during functional reorganization of adult visual cortex. *Nature Neuroscience*, 11(10), 1162–1167. <https://doi.org/10.1038/nn.2181>
- Kouser, M., Speed, H. E., Dewey, C. M., Reimers, J. M., Widman, A. J., Gupta, N., Liu, S., Jaramillo, T. C., Bangash, M., Xiao, B., Worley, P. F., & Powell, C. M. (2013). Loss of predominant shank3 isoforms results in hippocampus-dependent impairments in behavior and synaptic transmission. *Journal of Neuroscience*, 33(47), 18448–18468. <https://doi.org/10.1523/JNEUROSCI.3017-13.2013>
- Kreitzer, A. C., & Malenka, R. C. (2007). Endocannabinoid-mediated rescue of striatal LTD and motor deficits in Parkinson's disease models. *Nature*, 445(7128), 643–647. <https://doi.org/10.1038/nature05506>
- Lanciego, J. L., Luquin, N., & Obeso, J. A. (2012). Functional neuroanatomy of the basal ganglia. *Cold Spring Harbor Perspectives in Medicine*, 2, a009621. <https://doi.org/10.1101/cshperspect>
- Matas, E., Maisterrena, A., Thabault, M., Balado, E., Francheteau, M., Balbous, A., Galvan, L., & Jaber, M. (2021). Major motor and gait deficits with sexual dimorphism in a Shank3 mutant mouse model. *Molecular Autism*, 12(1), 2. <https://doi.org/10.1186/s13229-020-00412-8>
- Nelson, S. B., & Valakh, V. (2015). Excitatory/inhibitory balance and circuit homeostasis in autism spectrum disorders. *Neuron*, 87(4), 684–698. <https://doi.org/10.1016/j.neuron.2015.07.033>
- Nestler, E. J., & Hyman, S. E. (2010). Animal models of neuropsychiatric disorders. In *Nature Neuroscience* (Vol. 13, issue 10) (pp. 1161–1169). Nature Publishing Group. <https://doi.org/10.1038/nn.2647>
- Noone, S. J., Jones, R. S. P., & Hastings, R. P. (2006). Care staff attributions about challenging behaviors in adults with intellectual disabilities. *Research in Developmental Disabilities*, 27(2), 109–120. <https://doi.org/10.1016/j.ridd.2004.11.014>
- Obeso, J. A., Rodríguez-Oroz, M. C., Benitez-Temino, B., Blesa, F. J., Guridi, J., Marin, C., & Rodriguez, M. (2008). Functional organization of the basal ganglia: Therapeutic implications for Parkinson's disease. *Movement Disorders*, 23(SUPPL. 3), 548–559. <https://doi.org/10.1002/mds.22062>
- Owen, S. F., Berke, J. D., & Kreitzer, A. C. (2018). Fast-spiking interneurons supply feedforward control of bursting, calcium, and plasticity for efficient learning. *Cell*, 172(4), 683–695.e15. <https://doi.org/10.1016/j.cell.2018.01.005>
- Pchitskaya, E., & Bezprozvanny, I. (2020). Dendritic spines shape analysis—Classification or clusterization? Perspective. In *Frontiers in synaptic neuroscience* (Vol. 12) (31). Frontiers Media S. A. <https://doi.org/10.3389/fnsyn.2020.00031>
- Peça, J., Feliciano, C., Ting, J. T., Wang, W., Wells, M. F., Venkatraman, T. N., Lascota, C. D., Fu, Z., & Feng, G. (2011). Shank3 mutant mice display autistic-like behaviours and striatal dysfunction. *Nature*, 472(7344), 437–442. <https://doi.org/10.1038/nature09965>
- Peñagarikano, O., Abrahams, B. S., Herman, E. I., Winden, K. D., Gdalyahu, A., Dong, H., Sonnenblick, L. I., Gruver, R., Almajano, J., Bragin, A., Golshani, P., Trachtenberg, J. T., Peles, E., & Geschwind, D. H. (2011). Absence of CNTNAP2 leads to epilepsy, neuronal migration abnormalities, and core

- autism-related deficits. *Cell*, 147(1), 235–246. <https://doi.org/10.1016/j.cell.2011.08.040>
- Platt, R. J., Zhou, Y., Slaymaker, I. M., Shetty, A. S., Weisbach, N. R., Kim, J. A., Sharma, J., Desai, M., Sood, S., Kempton, H. R., Crabtree, G. R., Feng, G., & Zhang, F. (2017). Chd8 mutation leads to autistic-like behaviors and impaired striatal circuits. *Cell Reports*, 19(2), 335–350. <https://doi.org/10.1016/j.celrep.2017.03.052>
- Rojas, D. C., Peterson, E., Winterrowd, E., Reite, M. L., Rogers, S. J., & Tregellas, J. R. (2006). Regional gray matter volumetric changes in autism associated with social and repetitive behavior symptoms. *BMC Psychiatry*, 6, 1–13. <https://doi.org/10.1186/1471-244X-6-56>
- Rothwell, P. E., Fuccillo, M. V., Maxeiner, S., Hayton, S. J., Gokce, O., Lim, B. K., Fowler, S. C., Malenka, R. C., & Südhof, T. C. (2014). Autism-associated neuroligin-3 mutations commonly impair striatal circuits to boost repetitive behaviors. *Cell*, 158(1), 198–212. <https://doi.org/10.1016/j.cell.2014.04.045>
- Rubenstein, J. L. R., & Merzenich, M. M. (2003). Model of autism: Increased ratio of excitation/inhibition in key neural systems. *Genes, Brain and Behavior*, 2, 255–267. <https://doi.org/10.1046/j.1601-183X.2003.00037.x>
- Schoufour, J. D., Mitnitski, A., Rockwood, K., Evenhuis, H. M., & Echteld, M. A. (2013). Development of a frailty index for older people with intellectual disabilities: Results from the HA-ID study. *Research in Developmental Disabilities*, 34(5), 1541–1555. <https://doi.org/10.1016/j.ridd.2013.01.029>
- Sebastian, V., Estil, J. B., Chen, D., Schrott, L. M., & Serrano, P. A. (2013). Acute physiological stress promotes clustering of synaptic markers and alters spine morphology in the hippocampus. *PLoS ONE*, 8(10), e79077. <https://doi.org/10.1371/journal.pone.0079077>
- Thabault, M., Turpin, V., Maisterrena, A., Jaber, M., Egloff, M., & Galvan, L. (2022). Cerebellar and striatal implications in autism spectrum disorders: From clinical observations to animal models. *International Journal of Molecular Sciences*, 23(4), 2294. <https://doi.org/10.3390/ijms23042294>
- Varghese, M., Keshav, N., Jacot-Descombes, S., Warda, T., Wicinski, B., Dickstein, D. L., Harony-Nicolas, H., de Rubeis, S., Drapeau, E., Buxbaum, J. D., & Hof, P. R. (2017). Autism spectrum disorder: Neuropathology and animal models. *Acta Neuropathologica*, 134(4), 537–566. <https://doi.org/10.1007/s00401-017-1736-4>
- Wegiel, J., Flory, M., Kuchna, I., Nowicki, K., Yong Ma, S., Imaki, H., Wiegand, J., Cohen, I. L., London, E., Wisniewski, T., & Brown, W. T. (2014). Stereological study of the neuronal number and volume of 38 brain subdivisions of subjects diagnosed with autism. *Acta Neuropathologica Communications*, 2(141), 1–18.
- Yoo, T., Cho, H., Lee, J., Park, H., Yoo, Y. E., Yang, E., Kim, J. Y., Kim, H., & Kim, E. (2018). GABA neuronal deletion of Shank3 exons 14–16 in mice suppresses striatal excitatory synaptic input and induces social and locomotor abnormalities. *Frontiers in Cellular Neuroscience*, 12, 341. <https://doi.org/10.3389/fncel.2018.00341>
- Zampella, C. J., Wang, L. A. L., Haley, M., Hutchinson, A. G., & de Marchena, A. (2021). Motor skill differences in autism spectrum disorder: A clinically focused review. In *Current psychiatry reports* (Vol. 23, issue 10) (p. 64). Springer. <https://doi.org/10.1007/s11920-021-01280-6>
- Zurek, A. A., Kemp, S. W. P., Aga, Z., Walker, S., Milenkovic, M., Ramsey, A. J., Sibille, E., Scherer, S. W., & Orser, B. A. (2016). $\alpha 5$ GABAA receptor deficiency causes autism-like behaviors. *Annals of Clinical Translational Neurology*, 3(5), 392–398. <https://doi.org/10.1002/acn3.303>

How to cite this article: Thabault, M., Turpin, V., Balado, É., Fernandes-Gomes, C., Huot, A.-L., Cantereau, A., Fernagut, P.-O., Jaber, M., & Galvan, L. (2023). Age-related behavioural and striatal dysfunctions in Shank3^{ΔC/ΔC} mouse model of autism spectrum disorder. *European Journal of Neuroscience*, 57(4), 607–618. <https://doi.org/10.1111/ejn.15919>